Available online at www.sciencedirect.com
ScienceDirect
Nuclear Instruments and Methods in Physics Research A 576 (2007) 223–234
NUCLEAR INSTRUMENTS & METHODS IN PHYSICS RESEARCH Section A
www.elsevier.com/locate/nima

Data processing and image reconstruction methods for pixel detectors

Jan Jakubek*

Institute of Experimental and Applied Physics, Czech Technical University in Prague, Horska 3a/22, CZ 12800 Prague 2, Czech Republic

Available online 6 February 2007

Abstract

Semiconductor single-particle-counting pixel detectors offer many advantages for radiation imaging: high detection efficiency, energy discrimination, noiseless digital integration (counting), high frame rate and virtually unlimited dynamic range. All these properties allow to achieve high quality images. Examples of transmission images and 3D tomographic reconstruction using X-rays and slow neutrons are presented demonstrating effects that can affect the quality of images. A number of obstacles can limit detector performance if not handled. The pixel detector is in fact an array of individual detectors (pixels), each of them has its own efficiency, energy calibration and also noise. The common effort is to make all these parameters uniform for all pixels. However, an ideal uniformity can be never reached. Moreover, it is often seen that the signal in one pixel affects neighboring pixels due to various reasons (charge sharing, crosstalk, etc.). All such effects have to be taken into account during data processing to avoid false data interpretation. The main intention of this contribution is to summarize techniques of data processing and image correction to eliminate residual drawbacks of pixel detectors. It is shown how to extend these methods to handle further physical effects such as hardening of the beam and edge enhancement by deflection. Besides, more advanced methods of data processing such as tomographic 3D reconstruction are discussed. All methods are demonstrated on real experiments from biology and material science performed mostly with the Medipix2 pixel device. A brief view to the future of pixel detectors and their applications also including spectroscopy and particle tracking is given too.

PACS: 42.30.Wb; 87.59.Fm; 42.30.Rx; 87.58.Mj

Keywords: Pixel detector; Image reconstruction; Tomography; X-ray radiography; Neutron radiography; Phase contrast imaging

1. Introduction

Radiation imaging can be used for a broad scale of applications in various fields such as nuclear physics, material research, archeology, biology, medicine, etc. This article concentrates on transmission radiography and its applications.

In the classical transmission radiographic arrangement, the investigated specimen is penetrated by a collimated beam of radiation modifying its properties (intensity, particle composition, energy spectrum, direction of propagation, polarization, etc.). The radiation imaging detector is placed behind a specimen recording the modified beam properties.

Quality of the irradiating beam together with the performance of radiation imaging detector is crucial for amount of information about structure of the investigated specimen which can be retrieved.

2. Imaging radiation detectors for transmission radiography

The first transmission radiogram was measured by Wilhelm Conrad Röntgen X-raying his wife's hand in 1895 (see Fig. 1). As a radiation imager, he used X-ray sensitive photographic emulsion. At present also, imagers of this type are used. They have many advantages but one very important drawback is the need of chemical processing which prevents their use in on-line digital radiography.

2.1. Digital imaging detectors

There are two main approaches in the field of imaging detectors for transmission radiography with the digital output:

*Tel.: +420 22435 9181; fax: +420 22435 9392.
E-mail address: jan.jakubek@utef.cvut.cz.

0168-9002/$ - see front matter © 2007 Elsevier B.V. All rights reserved.
doi:10.1016/j.nima.2007.01.157

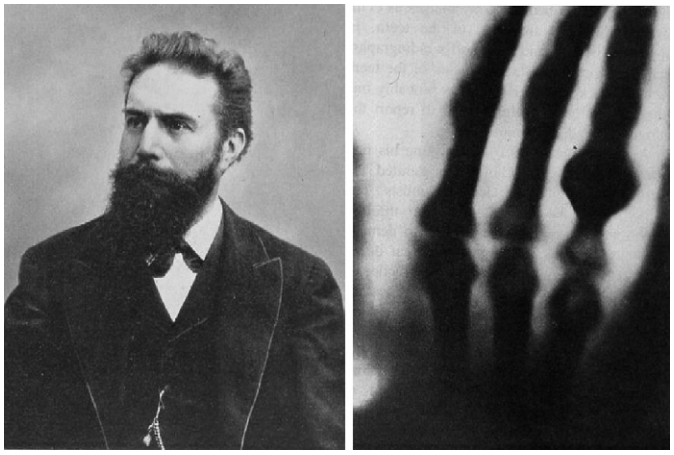

Fig. 1. Wilhelm Conrad Röntgen and X-ray radiogram of hand of his wife Anna Bertha taken in 1895.

(a) *Charge-integrating devices*: Ionizing radiation creates a charge which is collected and integrated in pixels (CCD, CMOS sensors, flat panels, etc.).
(b) *Particle-counting pixel detectors*: Ionizing particle creates a charge in a sensitive volume which is compared with a threshold, and digital counter is incremented.

As can be seen from Table 1, both approaches offer advantages and disadvantages making them suitable for different application fields. Generally speaking, charge-integrating devices are good for measurements with high radiation intensity. If radiation intensity is low then long exposure time is required for statistical noise suppression. With long exposure time, the contribution of the useful signal can be low in comparison with the integral of the so-called dark current which is always present in this type of devices. Therefore, the maximal signal-to-noise ratio (SNR) is limited.

2.2. Single-particle-counting pixel devices–semiconductor pixel detectors

In cases when the maximum count rate is lower than about 10^6 counts/pixel/s the particle-counting pixel detectors offer better results than charge-integrating devices. All false signals (leakage current and noise) are separated from the useful signal by threshold settings so that there is no false counting. Thus, dynamic range of pixel detectors is in fact unlimited and it is possible to reach almost arbitrary SNR just by exposure time prolongation.

The maximal count rate of 10^6 counts/pixel/s is more than sufficient for most radiographic applications. Moreover, new designs of pixel detectors such as Timepix [19] offer an ability of CCD like operation with a digital integration of charge quanta, which have energy higher than certain threshold level. There will be no dead time present in this mode and the limit of the maximal detectable intensity will be eliminated.

Table 1
Comparison of charge-integrating devices with particle counting pixel detectors

Charge-integrating devices	Particle-counting pixel detectors
High spatial resolution (~5 μm)	Good spatial resolution (~50 μm)
Zero dead time	Nonzero dead time
Not energy sensitive	Energy discrimination
Dark current	No dark current
Noise	No noise (separated by threshold)
Limited dynamic range	Unlimited dynamic range
Limited linearity	Ideal linearity (counting)

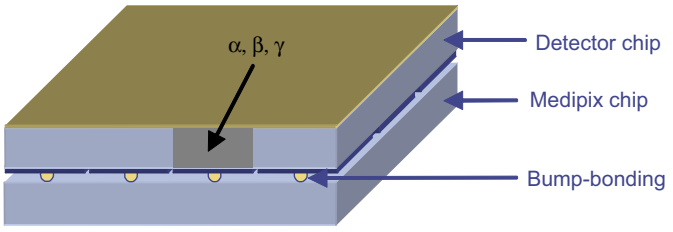

Fig. 2. Hybrid structure of Medipix2 device.

2.3. Semiconductor pixel device of Medipix2 type

The typical representative of a single quantum counting pixel imager designed for radiography is the Medipix2 device.

The hybrid silicon pixel device Medipix2 developed at CERN [1] was originally designed for position sensitive single X-ray photon detection. With appropriate sensor, the device can be used for registration of any type of ionizing particles. The device consists of a semiconductor detector chip (Si, GaAs, CdTe, HgI, etc.) bump bonded to a readout chip. The detector chip is equipped with a single common backside electrode and a front side matrix of electrodes (256×256 square pixels with pitch of 55 μm) as depicted in Fig. 2.

Each element of the matrix (pixel) is connected to its respective preamplifier, double discriminator and digital counter integrated on the readout chip. Block diagram of the pixel circuitry is shown in Fig. 3.

The communication frequency can be as high as 200 MHz allowing complete data readout in about 200 μs via 32-bit parallel or in 5 ms via serial interface.

The Medipix device is connected to PC by dedicated interface. There are several interface types allowing either high frame rate or good connectivity and portability. The whole setup (Medipix2 + interface) can be as small and portable as displayed in Fig. 4.

3. Transmission radiography with single-particle-counting pixel detectors

In the transmission radiography, the properties of a well-defined beam of radiation are modified by passing through a sample. Modified beam property is recorded by a suitable

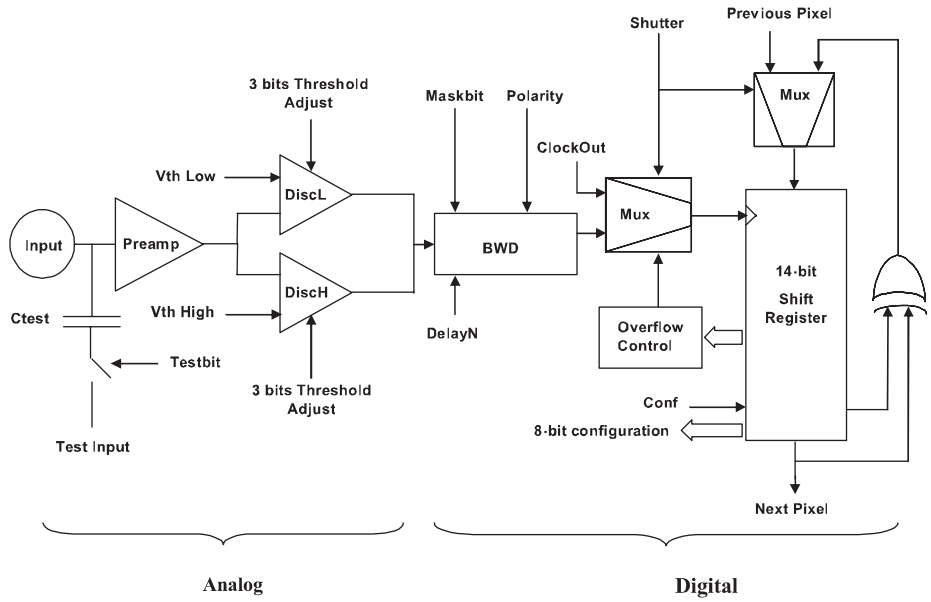

Fig. 3. Block diagram of single pixel cell of Medipix2 device type [1].

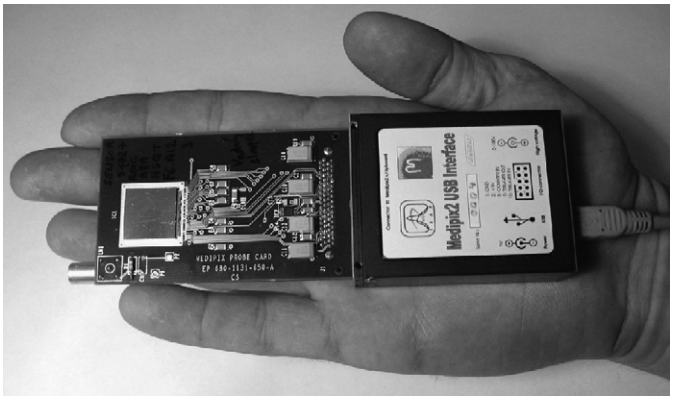

Fig. 4. Portable setup of Medipix2 device (left) with USB interface (right).

imaging detector. From obtained images the internal structure of the sample is estimated.

According to the type of radiation and its properties which are followed the domain of transmission radiography splits into many branches. Almost any kind of radiation can be used for transmission radiography (photons, charged particles, neutrons, ions) and almost any property can be followed (intensity, energy, polarization, direction, etc.).

3.1. X-ray transmission radiography

In X-ray transmission radiography intensity of the X-ray beam is attenuated by the object material. The imaging detector records changes in the beam intensity.

Typical sources of X-ray radiation are X-ray tubes providing polychromatic radiation and more rarely synchrotron facilities which can produce monochromatic radiation.

If a pixel photon counting pixel detector is used as imager its response has to be calibrated. The reason is that a detection efficiency of individual pixels is never uniform mainly due to differences in analog circuits integrated in the pixels. Thus, an interpixel constant pattern noise is introduced into the intensity images taken.

3.1.1. Flat-field correction

The simplest method suppressing image distortion due to pixel efficiency nonuniformity is the flat-field correction [2]. In the flat-field correction we assume that it is possible to find a matrix of multiplicative coefficients characterizing the relative efficiency of each pixel to the efficiency of an average pixel.

The matrix of flat-field correction coefficients $\boldsymbol{C}$ is obtained from measurement in a flat irradiation field (all pixels are irradiated by the same intensity) taking the so-called *flood* image $\boldsymbol{F}$. Count $f_{i,j}$ detected by i,jth pixel should be ideally equal to the mean value $\bar{f}$ of all pixels. Correction coefficient for i,jth pixel is computed using $c_{i,j} = \bar{f}/f_{i,j}$.

The mean value $\bar{f}$ can be computed either theoretically or estimated from measured data, e.g., as average or (better) as median of all $f_{i,j}$.

The image $\boldsymbol{R}$ (raw image) of an unknown sample can be corrected via a per pixel multiplication of the measured pixel value $r_{i,j}$ and its respective correction coefficient $c_{i,j}$ producing the final image $\boldsymbol{V}$ with i,jth pixel $v_{i,j} = c_{i,j}r_{i,j}$ (Fig. 5).

3.1.2. Polychromatic irradiation and beam hardening effect

The attenuation of X-ray beam intensity in a material depends on the beam energy as well as on the material properties. Therefore, in case of polychromatic irradiation, each energy fraction of the incident beam is attenuated

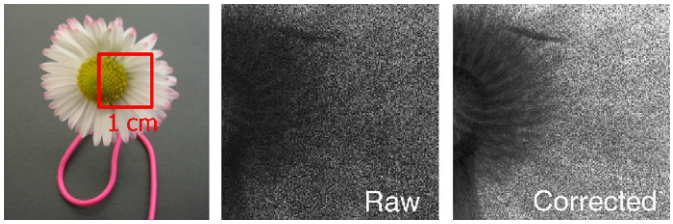

Fig. 5. Photograph, raw image and flat-field corrected image of daisy blossom. As a polychromatic X-ray irradiation was used, the corrected image is still imperfect due to the beam-hardening effect.

with different attenuation coefficient. Generally, it can be stated that harder components of spectrum are attenuated less than softer components. This effect is often called *Beam Hardening* (BH). If attenuation in the investigated object is not homogenous (e.g. its thickness varies) then the transmitted beam spectrum differs from point to point. Simply speaking, behind thicker parts of the sample the spectrum is harder than behind thinner parts. If the pixel detector is used for intensity image recording, then individual pixels are irradiated by different spectrum.

The detection efficiency of pixels is unfortunately energy dependent and, moreover, this dependence is unique for each of them (see Fig. 6). This means that the detection efficiency of pixels depends individually on the local attenuation properties of the sample and thus, the method of flat-field correction is not sufficient.

One technique of correction of the differences between pixels is based on the assumption that material composition of the object is "good". Ideally, it would be the sample composed of a single material just with different density.

With this assumption one can use the *Signal-to-equivalent Thickness Calibration* (STC) method [3]. The calibration is performed with a set of flat and homogenous absorbers ideally with identical material composition as the sample. The dependence of the detected count rate on the absorber thickness is measured (calibrated) for each pixel. Thus, for i,jth pixel the calibration function $h_{i,j}$ is measured. This function translates the count rate into equivalent thickness.

The image $\boldsymbol{R}$ of an unknown sample can be then corrected by assignment of equivalent thickness to each pixel forming a new image $\boldsymbol{B}$. The i,jth pixel in the corrected image $\boldsymbol{B}$ is computed as $b_{i,j} = h_{i,j}(r_{i,j})$.

The described correction method works well even for slightly different calibrating and sample materials as illustrated in Fig. 7.

The calibration function $h_{i,j}$ is determined by measurement in a discrete set of points (measured count rates y_k at thicknesses x_k for $k = 1, \ldots, n$). Its value has to be computed by interpolation between these points.

A proper interpolation model is based on locally exponential fit (see Figs. 8 and 9). In this case, it is assumed that in each point the function can be locally

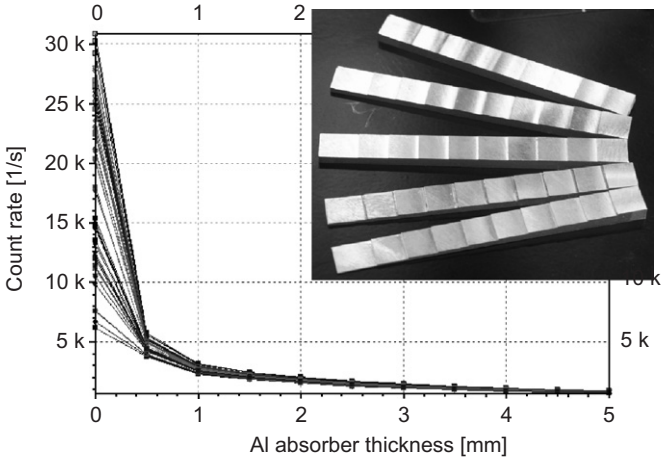

Fig. 6. Count rates detected by several pixels (each line characterizes one pixel) in dependence on aluminum absorber thickness. Samples were irradiated by a tungsten X-ray tube at 70 kV. Aluminum tiered samples used for this measurement are displayed in the inset.

approximated by an exponential function with offset:[1]

$$y = h^{-1}(x) = A_k\, e^{a_k x} + O_k.$$

Such fit is done in each calibration point $(1,\ldots, n)$. A sequence of parameters A_k, a_k and O_k $(k = 1,\ldots, n)$ is created for each pixel. The measured value y is then corrected using term

$$h(y) = \frac{y - y_{k+1}}{a_k(y_k - y_{k+1})} \ln\frac{y - O_k}{A_k} + \frac{y_k - y}{a_{k+1}(y_k - y_{k+1})} \ln\frac{y - O_{k+1}}{A_{k+1}}$$

where k is the calibration point index for which the condition $y_k > y > y_{k+1}$ is valid.

A significant advantage of the described correction method is the linearization of the measured data as illustrated in Fig. 10. This feature is very important for data processing using algorithms of computed tomography (CT).

3.2. X-ray CT

X-ray CT, first introduced by Cormack and Hounseld (1963), is an X-ray imaging modality that enables the generation of cross-sectional slices of an object, often the human body. Today, X-ray CT continues to be one of the leading clinical imaging modalities. For the computed tomography a CT scanner records object projections at many different angles. From these data a 3D image of the object structure is computed.

There is a variety of methods to reconstruct clinically useful 3D images from CT measurements. The most

[1]This assumption is based on the following simplification. In a very small range of thicknesses, some photons (hard fraction) are not attenuated at all making a constant background O, some (soft fraction) are fully attenuated and remaining photons are attenuated following exponential law Ae^{ax}. Then the total attenuation function is $Ae^{ax} + O$.

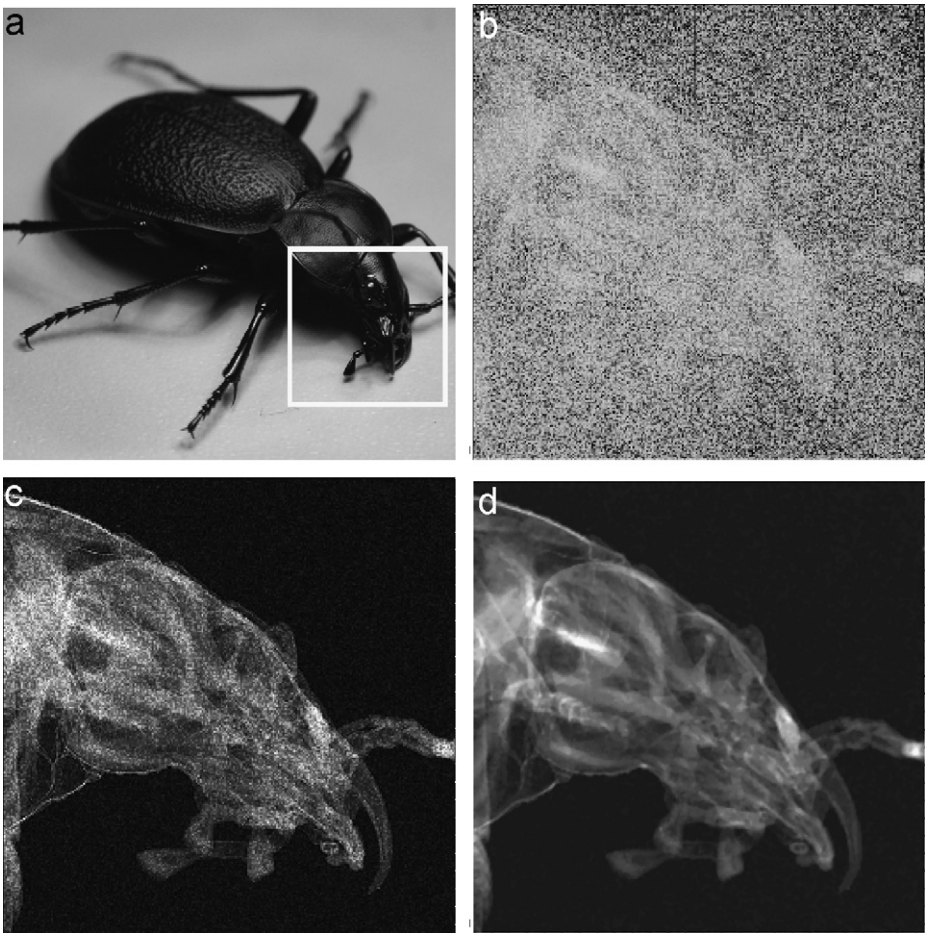

Fig. 7. Ground beetle: photograph (a), X-ray transmission image—raw data (b), the same image corrected by flat-field correction where thick parts are noisy due to beam hardening effect (c) and the image corrected by signal-to-thickness calibration technique using a set of three aluminum foils for calibration (d).

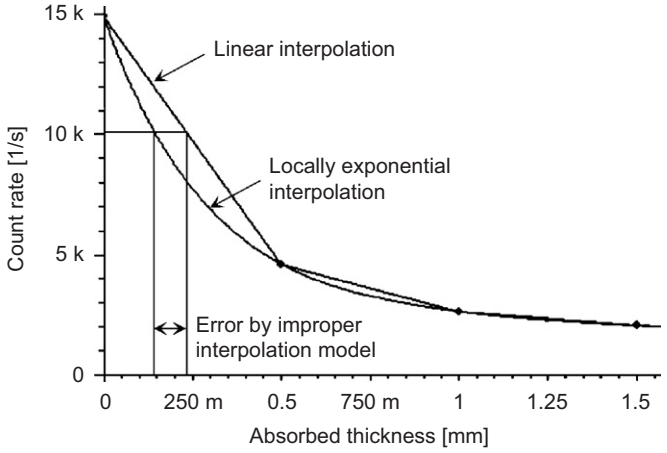

Fig. 8. Inverted calibration function h^{-1} for a single pixel. Function values were measured at four points and interpolated in between. Incorrect interpolation model (e.g. linear) can lead to a large error.

dominant CT reconstruction technique is *Filtered Back Projection* (FBP) method [4]. FBP is analytic and its practical implementations take advantage of the *Fast Fourier Transform* (FFT). FBP is fast and deterministic and its properties are well understood. However, FBP is fully correct only when the noise influence can be neglected and when the number of projections is infinite which in real experiments is hardly achievable.[2] Moreover, it is difficult to incorporate more elaborate physical models into the FBP method (complex geometry, influence of scattering, fluorescence, beam hardening, phase effects, etc.). Therefore, FBP can lead to artifacts in reconstructed images.

Another approach uses an iterative scheme of tomographic reconstruction. A typical algorithm which uses iterative approach is based on *Expectation Maximization* (EM) [5].

In the first iteration the uniform "trial" object is taken into account and its projections are computed (using even a very sophisticated physical model). The projections obtained are compared with those acquired by measurement. Using this comparison the trial object is modified to produce projections which are closer to the measured data. Then the algorithm iteratively repeats. The trial object is modified in each iteration and its projections converge to measured data. The main disadvantage of the iterative

[2]This is true especially in case of low statistics measurements such as PET or SPECT. In the case of X-ray CT, the FBP is usually sufficient.

approach are the high computational requirements. A single iteration demands usually the same power as two full reconstructions in FBP.

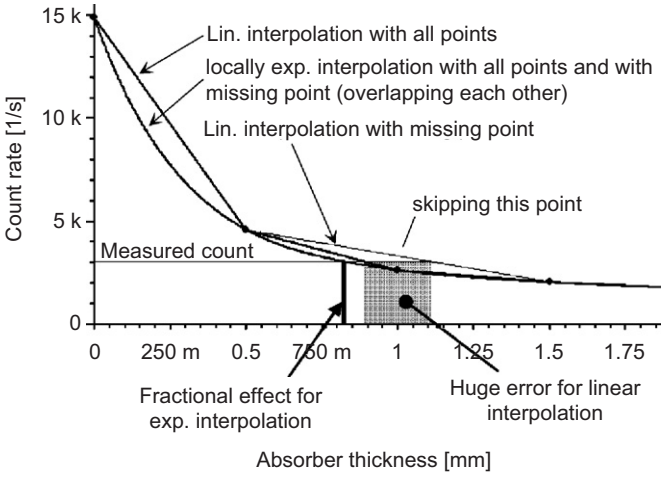

Fig. 9. Correct interpolation scheme is less sensitive to missing points.

To accelerate convergence speed of iterative algorithms a technique of *Ordered Subsets* (OS) can be used [6]. When combined with the EM method it is called OSEM. OS technique splits each iteration into several subiterations. In each subiteration just a selected subset of all projections is used for trial object modification. The following subiteration uses a different subset of projections and so on. After all projections are used, the single full iteration is finished. The number of projections in each subset can be as low as 3 or 4 (OSEM method is then labeled OSEM3 or OSEM4). The speed of an iterative process is multiplied by number of subsets used (with some remarks).

Iterative methods are advantageous when the projection data are noisy, when the number of projections is low (illustrated in Fig. 11) and when the physical model is too complex.

For most CT reconstruction algorithms it is necessary to preprocess the measured transmission data to be made linearly dependent on the object absorption. For monochromatic radiation, the dependence is exponential and can be linearized taking the logarithm of the data. In the

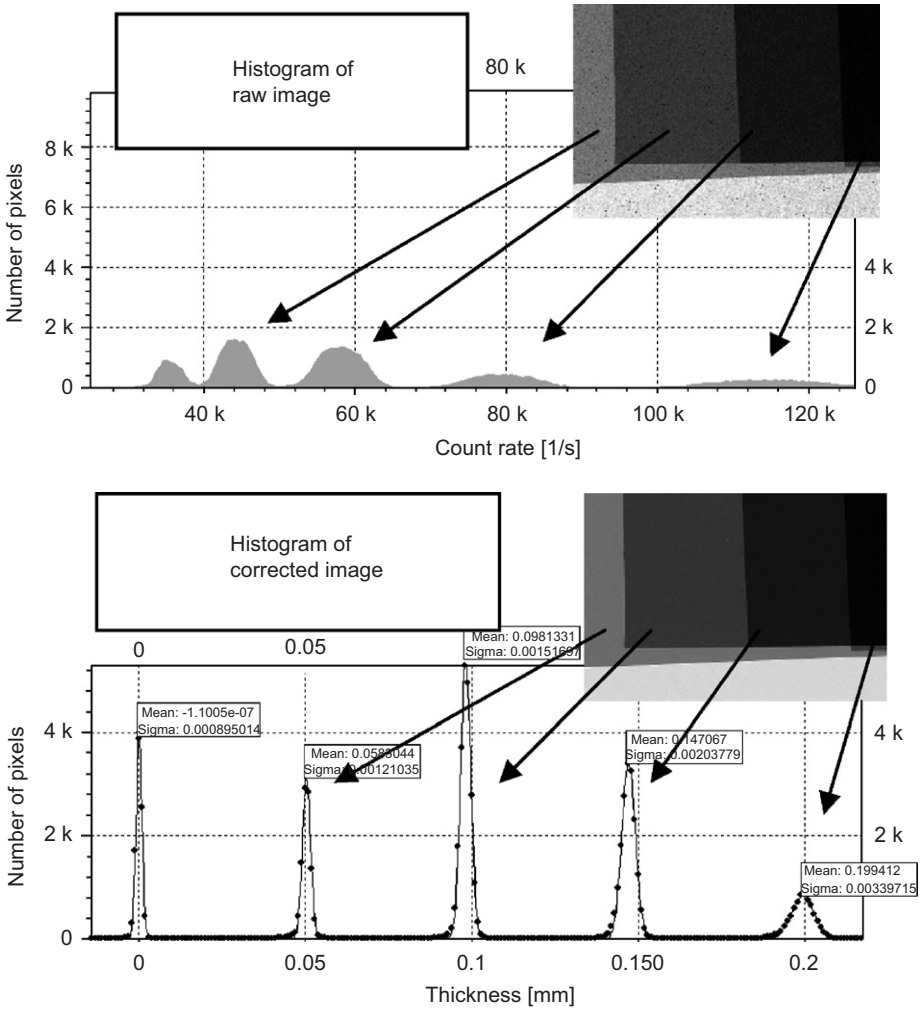

Fig. 10. Histogram of raw image of overlapping 50 μm thick aluminum foils (top) and histogram of corrected image (bottom). Peaks in the second histogram are narrow and equidistant (linearization feature).

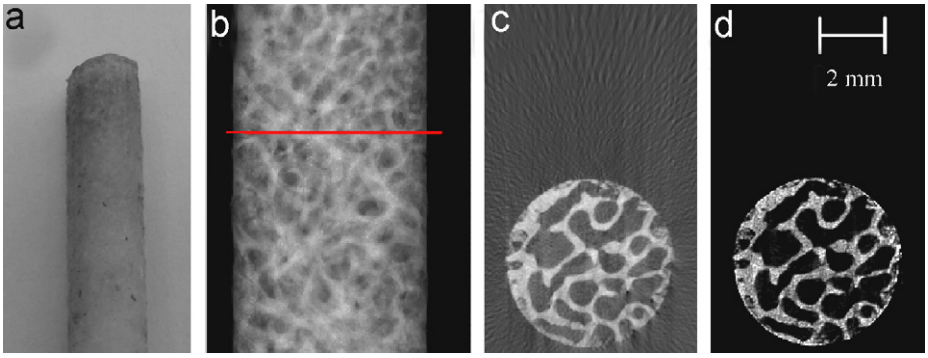

Fig. 11. Cylindrical bone cut (cow): Photograph (a), single projection with slice position indicated by line (b), FBP reconstruction of a single slice with streak artifacts caused by low number of projections (c) and OSEM3 reconstruction of the same slice (d). Reconstructions done from 90 projections measured with tungsten X-ray tube at 40 kV.

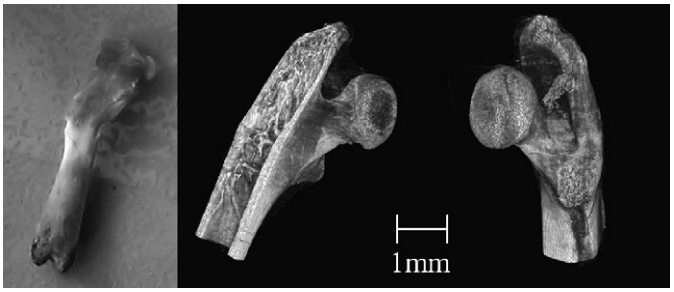

Fig. 12. Reconstructed structure of fresh mouse innominate bone performed by three iterations in OSEM3 method from 90 projections measured with tungsten X-ray tube at 70 kV.

polychromatic case (X-ray tube as source) the dependence is generally unknown.

Pixel detectors equipped with an appropriate sensor chip (Si for small or light objects, e.g. soft tissue, GaAs or CdTe for larger or heavier objects) are well suited for CT. The measured projections can be linearized using technique described in Section 3.1.2. It has to be emphasized that this linearization method is fully precise just for ideal material composition of the object (soft tissue is fine from this point of view).

Several examples of CT reconstructions by OSEM algorithm from data measured by the Medipix device with 300 μm thick silicon sensor and a microfocus X-ray tube are shown in Figs. 12 and 13.

3.3. In-line phase contrast imaging with X-rays

In addition to absorption effect, the changes of the transmitted wave phase can be observed under some circumstances and exploited for imaging purposes.

The phase of spatially coherent X-ray waves passing an object is shifted according to effective refractive index. The effective refractive index is integral of refractive index along the propagation direction of the X-rays. Variations in the effective refractive index cause variations in the phase of transmitted waves. This phase shift deforms the wavefront of the transmitted radiation in a way that the rays are deflected from their original propagation direction and a loss of intensity is detected in a forward direction. This process causes edge enhancement in the obtained image [7] (see Fig. 14). The technique can be used with monochromatic and even polychromatic X-ray source [8].

A substantial advantage of such imaging method is that X-ray photons used for phase contrast imaging have to be able to penetrate through a sample (so they should have sufficient energy) and therefore they do not contribute to radiation dose [9].

If a microfocus X-ray tube is used as a X-ray source then transversal coherence is assured by the small size of the focal spot.

Since a deflection angle α is very small (micro radians) the object to detector distance L (see Fig. 15) has to be large enough to resolve phase contrast effects. The required distance depends on pixel size, beam energy, object composition and size (for 55 μm pixel size, 20 keV X-rays and small soft tissue object, L should be at least 50 cm). At such distances, microfocus X-ray tubes cannot provide high beam intensity. Therefore charge-integrating devices are not suitable for phase contrast imaging. Usage of a highly sensitive and noiseless imaging sensor of Medipix2 type is advantageous as illustrated in Figs. 16 and 17.

The signal caused by phase effects can be for light and therefore almost transparent samples many times larger than signal caused by absorption (see Fig. 18).

The energy dependence of the refractive index differs from the energy dependence of absorption. As Medipix device offers capability of energy discrimination it is possible to distinguish whether images are affected by phase shift effects or not.[3] If two images of the same object are measured at two different energy discrimination levels and both images are translated into equivalent thicknesses[4]

[3] If there is no other energy dependent influence.

[4] Translation is done using signal to thickness calibration method described in Section 3.1.2. Calibration has to be done for each discrimination level separately.

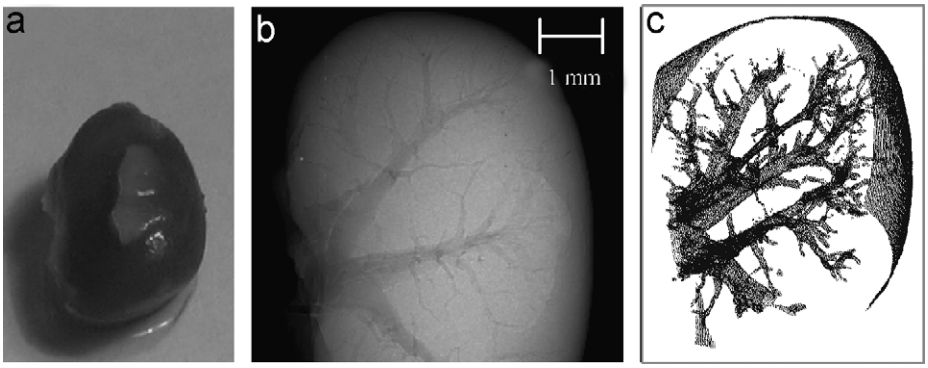

Fig. 13. Mouse kidney: photograph (a), single projection (b) and 3D reconstruction (c). Reconstructions performed by three iterations in OSEM3 method from 72 projections measured with tungsten X-ray tube at 40 kV.

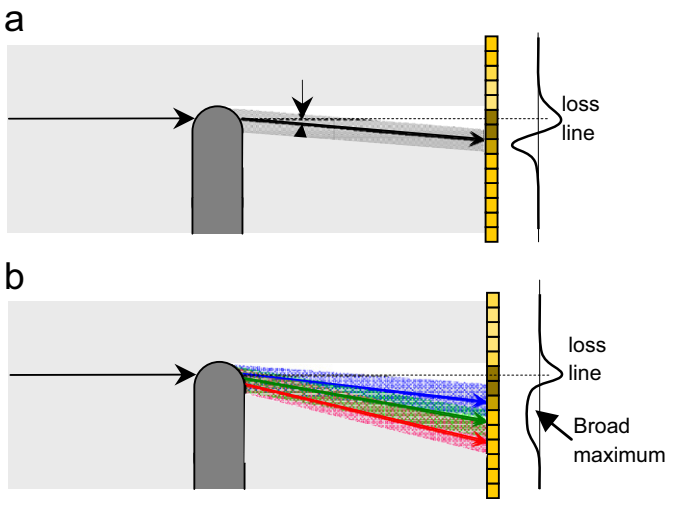

Fig. 14. Principle of in-line phase contrast imaging. Deflection of the beam results in change of intensity profile of the transmitted beam.

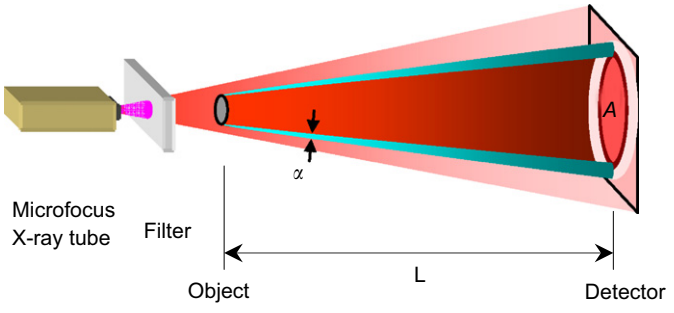

Fig. 15. Setup for in-line phase contrast imaging with microfocus X-ray tube. Distance L has to be large to distinguish small deflection angle α.

then the absorption information contained in both images can be suppressed by their subtraction as shown in Fig. 19.

A pure phase image and a pure absorption image can be recovered from a pair of images taken with different energy discrimination as described in [10]. For this method the pixel detector with a pair (or more) of independent discriminators and counters would be advantageous, Medipix3 for example [11].

3.4. Transmission radiography and phase enhanced imaging with slow neutrons

The principle of neutron transmission radiography is identical to X-ray radiography: the intensity of neutron beam is attenuated by the object material and then recorded by a neutron sensitive imaging detector.

Thanks to different values of neutron and X-ray attenuation coefficients in matter, neutron radiography can visualize structures which can be hardly distinguished with X-rays (e.g. light elements such as hydrogen or carbon in plastic or biological samples).

One example is given by the images of a blank shell (cartridge) displayed in Fig. 20. The rather massive brass container is (in contrast to the explosive filling) essentially transparent to the neutron beam. Conversely, the attenuation of X-rays by the explosive is negligible in comparison to the attenuation by the casing. Thus, while the roentgenogram shows a seemingly empty container, the neutronogram reveals the presence of the explosive filling.

Adapting a pixel detector for detection of slow neutrons requires the use of a suitable neutron converter material. Converter material captures slow neutrons and produces secondary radiation which can be detected by the sensor chip. The range of secondary radiation in the sensor should be short to conserve high spatial resolution. Materials containing ^{6}Li or ^{10}B are well suited from this point of view as they convert neutrons to heavy charged particles.

The physical placement of the converter material can significantly affect the detection efficiency. The converter material can be deposited on the sensor surface [12], it can be inserted into pores in the sensitive volume of the detector [13] or it can be part of the semiconductive material itself [14,15].

Several examples of neutronographic images and tomographic reconstructions taken by the Medipix2

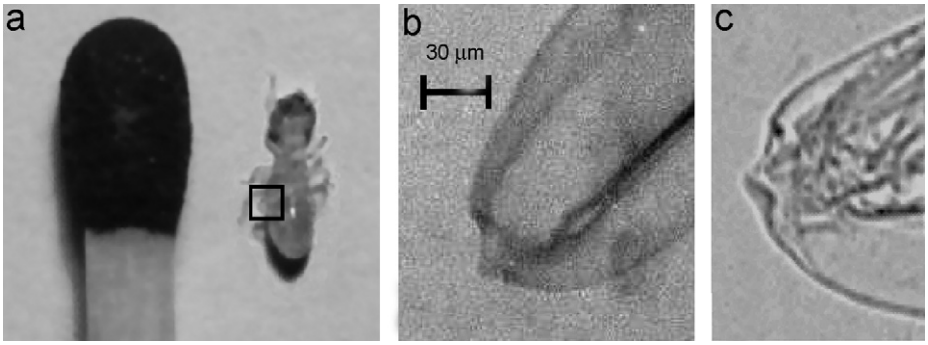

Fig. 16. Photograph of a termite worker (a), X-ray absorption image of termite knee taken by CCD with thin scintillator in contact geometry (b) and image with edges enhanced by phase contrast taken with Medipix2 (c) at distance of 60 cm revealing fine internal structure (Tungsten X-ray tube, 40 kV).

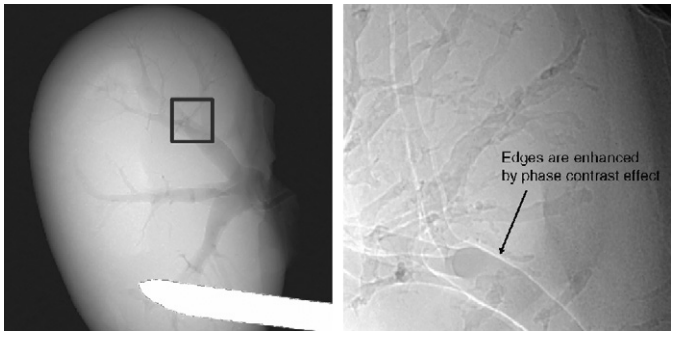

Fig. 17. X-ray transmission image of a mouse kidney (left). Enlarged area with edges enhanced by phase contrast (Medipix2, Tungsten X-ray tube, 40 kV).

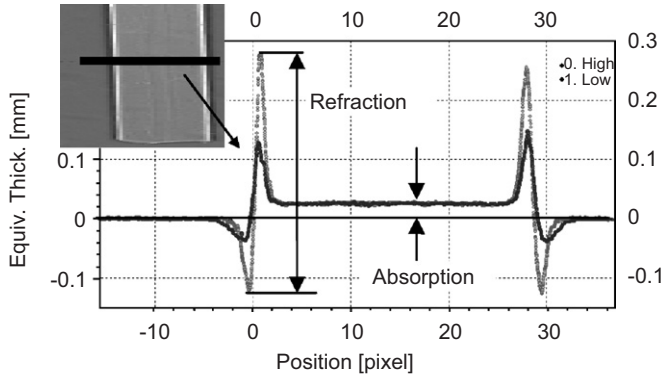

Fig. 18. X-ray image of a 0.5 mm thick polyethylene foil strip (inset) and its intensity profiles along the highlighted line measured with microfocus tungsten X-ray tube at 40 kV and Medipix2 detector (object to detector distance was 70 cm). Two measurements were done with different discrimination levels (7 and 11 keV). Refraction effects are of higher importance than absorption effects for higher X-ray energies.

device with silicon sensor coated with ^{6}LiF layer are shown in Figs. 21–23. Measurements were done at the NEUTRA station [16] of Paul Scherrer Institute in Switzerland. Spatial resolution in these images was about 100 μm in FWHM of line spread function.

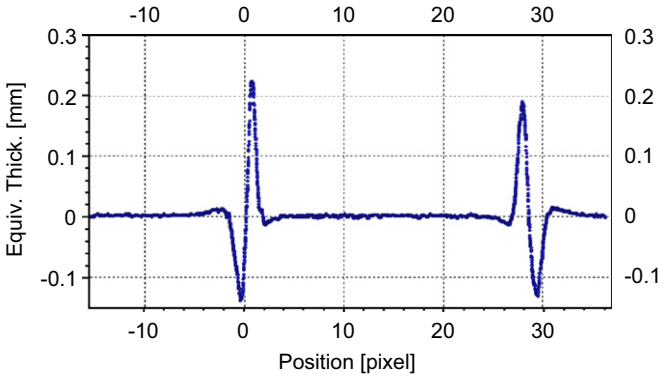

Fig. 19. Subtraction of profiles from Fig. 18. Signal caused by absorption is suppressed. Regions affected by phase shift are highlighted.

In neutron transmission radiography the effect of phase contrast enhancement can be exploited too. The effect is illustrated in Fig. 24 where the edges of two aluminum blocks are watched. Beam of cold neutrons at the ICON facility of PSI [17] and Medipix2 detector coated with ^{6}LiF converter were used.

3.5. Transmission radiography with heavy charged particles

Not only the intensity of radiation beams can be used for radiography. If the beam consists of monoenergetic heavy charged particles (protons, alphas, etc.) then their energy decreases by penetration through material as depicted in Fig. 25. Therefore, the structure of the object can be imaged by measurement of the energy loss of individual particles.

Is it possible to measure energy of heavy charged particle with a particle-counting pixel detector? Answer is yes. We can use several methods.

3.5.1. Energy determination using charge sharing effect

While heavy charged particles deposit their energy close to the sensor surface the ionization charge has to be collected to pixelated electrode through the full sensor thickness. Due to charge diffusion the charge cloud

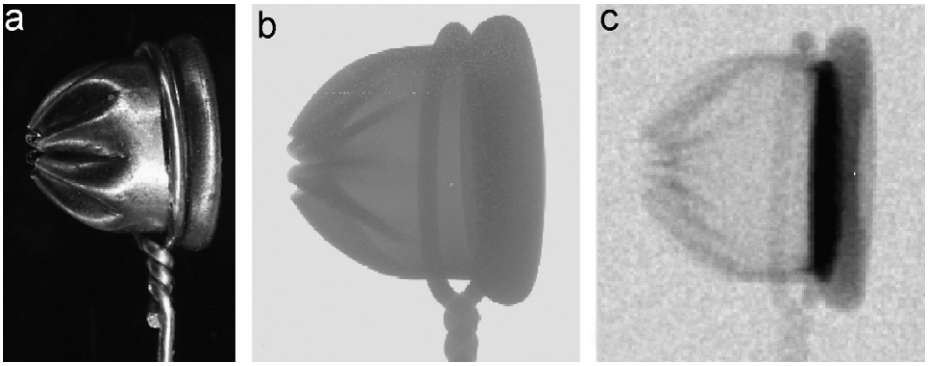

Fig. 20. Blank cartridge: photograph (a), X-ray radiogram (b) and neutron radiogram (c) revealing the presence of explosive filling. Radiograms taken by Medipix2 device.

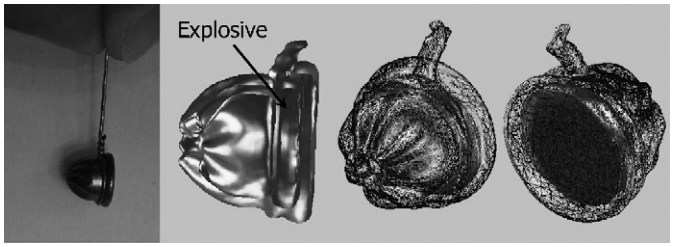

Fig. 21. Photograph and neutron tomographic 3D reconstructions of a blank cartridge (from 100 projections). Explosive filling is clearly visible.

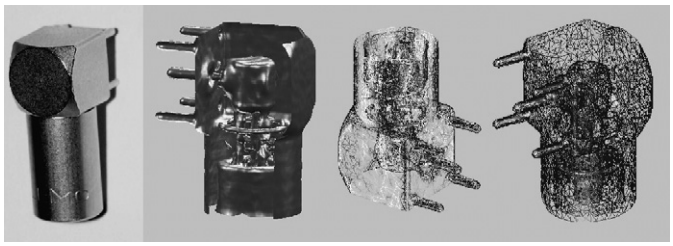

Fig. 22. Photograph and neutron tomographic 3D reconstructions of a LEMO connector (from 100 projections).

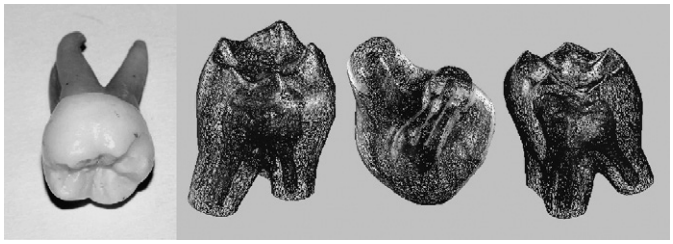

Fig. 23. Photograph and neutron tomographic 3D reconstructions of a fresh tooth.

expands and can spread even over several adjacent pixels. Each pixel compares the collected charge with some threshold level and counts if the charge is large enough. The single heavy charged particle is in such case counted by several adjacent pixels forming a cluster of pixels with signal (see Fig. 26).

The number of pixels in a cluster (cluster size) depends on the energy of detected particle. The sub pixel spatial resolution of interaction point can be reached by computation of a cluster centroid.

A very simple test of this method for radiography via measurement of energy loss was performed. The ^{241}Am isotope was used as source of monochromatic alpha particles (5.5 MeV) irradiating an object consisting of mylar foils lying directly on the Medipix2 detector surface. The dependence of cluster size (1000 clusters averaged) on mylar foil thickness was measured (Fig. 27). This dependence proves that cluster size can be used as a measure of particle energy and implicatively of foil thickness. The precision of thickness determination from average cluster size (1000 clusters) reaches 60 nm even in such a simple experiment.

Result of radiographic measurement of a wing of a fly in the same experimental setup is displayed in Fig. 28.

3.5.2. *Energy determination from back side pulse spectrometry*

While the charge created by heavy charged particle in a sensor chip is being collected the current pulse can be detected also in the backside contact of the sensor (in the common, not pixelated electrode). This mechanism can be used with Medipix2 detector and its USB interface for energy measurement and trigger generation [18]. Achieved energy resolution for 5.5 MeV alpha particles can be 30 keV in terms of FWHM.

3.5.3. *Direct energy measurement in each detector pixel*

New concepts of pixel detectors are becoming available. A direct Medipix2 successor called Timepix [19] offers the capability to use counter and comparator inside each pixel as a Wilkinson type ADC. Thus charge collected by each pixel is measured directly and the backside pulse signal can serve just as trigger.

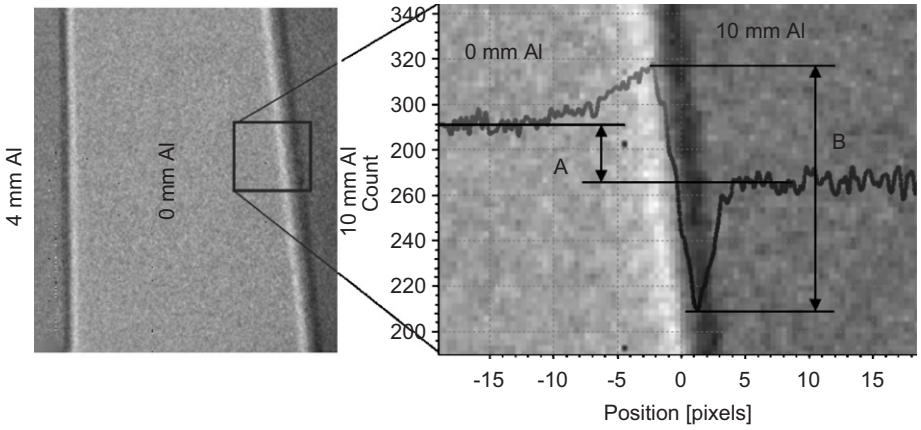

Fig. 24. Neutronogram of edges of two aluminum blocks: 4 mm thick (left) and 10 mm (right). The signal caused by phase contrast enhancement (B) is significantly larger than the absorption signal (A).

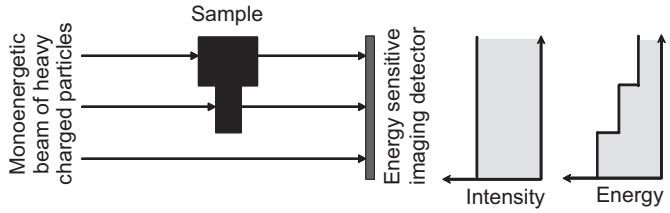

Fig. 25. Principle of radiography based on measurement of energy loss of heavy charged particles penetrating an investigated object.

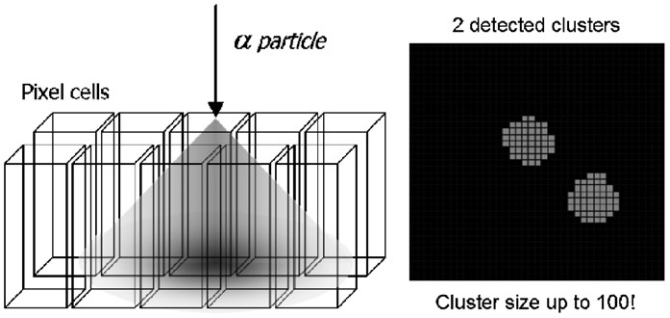

Fig. 26. Due to charge sharing effect a cluster of adjacent pixels arises a signal caused by a single heavy charged particle interaction.

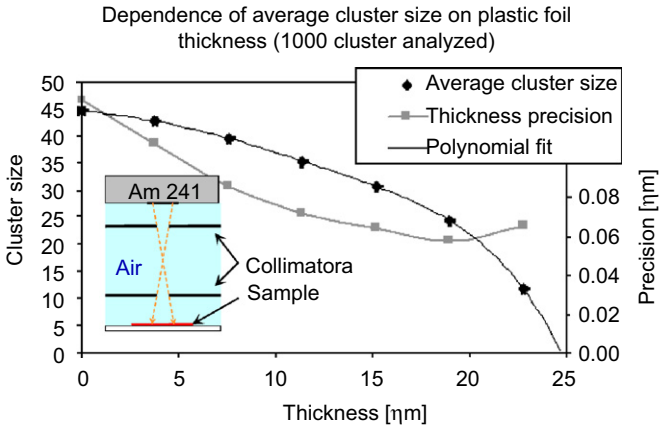

Fig. 27. Dependence of average cluster size on mylar foil thickness (dark curve, left vertical axis) and dependence of precision of foil thickness determination by cluster size measurement (gray curve, right vertical axis).

4. Future of single quantum counting pixel detectors

The amount of information which can be obtained from individual pixels is significant. Future pixel devices will provide more data, work faster and perform more sophisticated signal processing in each pixel. In the near future the two direct Medipix2 successors will follow such directive: Timepix [19], offering per pixel measurement of particle energy or its interaction time, and Medipix3 [11] having two independent counters allow simultaneous acquisition of two images with different energy threshold.

The signal taken from the backside contact of the sensor chip opens further possibilities of exploitation. For instance, this signal can be used for trigger generation or energy measurement (contact can be segmented to strips or superpixels to optimize noise properties or to estimate region of interest for optimized image readout).

Event-by-event measurement mode is a very powerful tool. It is often possible to determine the type of detected radiation by analysis of tracks caused by individual ionizing particles. From this point of view the pixel detector acts as a digital emulsion similar to former cloud or bubble chambers (see Fig. 29) [20]. The availability of such compact and portable device with functionality of a bubble chamber opens exploitation in many fields, e.g. for homeland security. But, the data readout and image analysis in an event-by-event mode increases the dead time significantly. Therefore, hardware has to be optimized for *Region of Interest* (ROI) readout and for the on-line data evaluation.

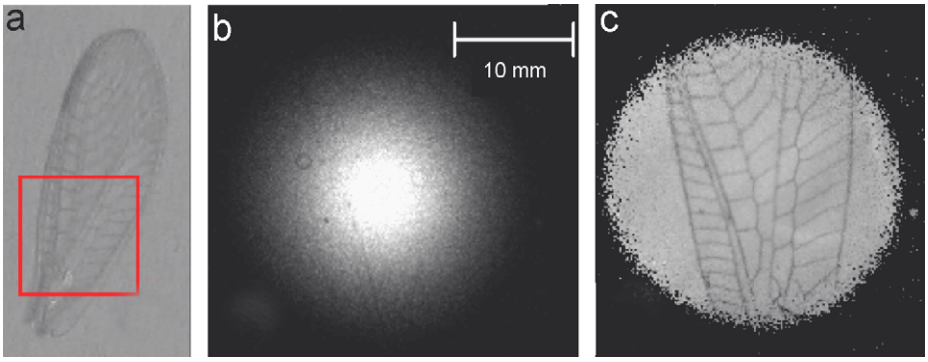

Fig. 28. Wing of a fly: photograph (a), intensity of transmitted alpha particles carrying no object related information (b) and average energy (in terms of cluster size) of transmitted alpha particles showing the object structure (c).

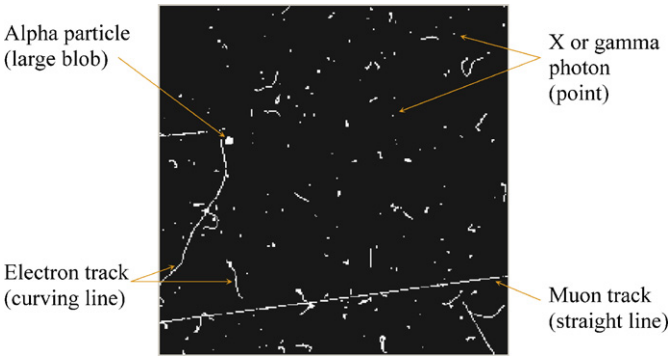

Fig. 29. Sample measurements of the natural background radiation with Medipix2 device with 700 μm Si sensor (10 min exposure time). Many electron tracks, one alpha particle cluster and rare cosmic muon track transversing sideways the sensor are identified.

Acknowledgments

This work has been carried out in frame of the CERN Medipix2 collaboration and has been supported in part by Research Grant *Collaboration of Czech Republic with CERN* No. 1P04LA211, by the *Fundamental Research Center* Project LC06041 of the *Ministry of Education, Youth and Sports of the Czech Republic*, by Project 1H-PK2/05 of the *Czech Ministry of Trade and Industry* and by Grant No. 106/04/0567 of the *Grant Agency of the Czech Republic*.

References

[1] X. Llopart, M. Campbell, R. Dinapoli, D. San Segundo, E. Pernigotti, Medipix2, a 64k pixel readout with 55 um square elements working in single photon counting mode, IEEE Trans. Nucl. Sci., NS-49 (2001) 2279–2283, in: Proceedings of the Conference Records of IEEE Nuclear Science Symposium and Medical Imaging Conference, San Diego, CA, 4–10 November 2001.

[2] L. Tlustos, Performance and limitations of high granularity single photon processing X-ray imaging detectors, PhD Thesis, University of Technology, Vienna ,CERN-THESIS-2005-032.

[3] D. Vavřík, J. Dammer, T. Holý, J. Jakůbek, S. Pospíšil, Z. Vykydal, Direct thickness calibration: way to radiographic study of soft tissues, in: M. Barone, et al., (Ed.), Proceedings of the 9th ICATPP Conference on Astroparticle, Particle, Space Physics, Detectors and Medical Physics Applications, Como Italy, October, 2005, World Scientific, 2006, in print.

[4] G.N. Ramachandran, A.V. Lakshminarayanan, Proc. Natl. Acad. Sci. 68 (1971) 2236.

[5] B.F. Hutton, J. Comput. Assist. Tomography 8 (2) (1984) 306.

[6] H.M. Hudson, R.S. Larkin, IEEE Trans. Med. Imag. 13 (4) (1994) 601.

[7] R. Fitzgerald, Phys. Today July (2000).

[8] S.W. Wilkins, et al., Nature 384 (1996) 335.

[9] T.J. Davis, et al., Nature 373 (1995) 595.

[10] J. Jakubek, et al., Compact system for high resolution X-ray transmission radiography, in-line phase contrast imaging and micro CT of biological samples, in: Conference record of Nuclear Science Symposium IEEE 2006, San Diego, October–November 2006.

[11] R. Ballabriga, M. Campbell, E.H.M. Heijne, X. Llopart, L. Tlustos, The Medipix3 prototype, a pixel readout chip working in single photon counting mode with improved spectrometric performance, in: Conference Record of Nuclear Science Symposium IEEE 2006, San Diego, October–November 2006.

[12] J. Jakůbek, T. Holý, E. Lehmann, S. Pospíšil, J. Uher, J. Vacík, D. Vavřík, Spatial resolution of the Medipix-2 as neutron pixel detector, in: Proceedings of the 6th IWORID, Instruments and Methods in Physics Research Section A, vol. 546, Issues 1–2, 1 July 2005, pp. 164–169, available on-line.

[13] J. Uher, C. Fröjdh, J. Jakůbek, C. Kenney, Z. Kohout, V. Linhart, S. Parker, S. Petersson, S. Pospíšil, G. Thungström, Highly sensitive silicon detectors of thermal neutrons, in: Conference Record of Nuclear Science Symposium IEEE 2006 San Diego, Octoberndash; November 2006.

[14] J. Jakubek, G. Mettivier, M. Cristina Montesi, S. Pospisil, P. Russo, J. Vacik, CdTe hybrid pixel detector for imaging with thermal neutrons, in: Contribution to the 7th IWORID, 4–7th July 2005, Grenoble, France. Nucl. Instr. Meth. A (2006), Available on-line at ⟨http://www.sciencedirect.com⟩.

[15] M. Schieber, M. Roth, A. Zuck, O. Khakhan, Z.B. Alfassi, Polycrystalline boron nitride based alpha and neutron detectors, in: Conference record of 15th International Room Temperature Semiconductor Detector Workshop IEEE 2006, San Diego, October–November.

[16] Paul Scherrer Institute web site: The Neutron Transmission Radiography (NEUTRA) Station at PSI at ⟨http://neutra.web.psi.ch/facility/index.html⟩.

[17] Paul Scherrer Institute web site, ICON—Imaging with Cold Neutrons at ⟨http://neutra.web.psi.ch/facility/icon_index.html⟩.

[18] Z. Vykydal, J. Jakubek, M. Platkevic, S. Pospisil, Nucl. Instr. and Meth. A 44785 (2006) available on-line at http://www.sciencedirect.com.

[19] Medipix collaboration web site at ⟨http://medipix.web.cern.ch/MEDIPIX/⟩.

[20] Z. Vykydal, J. Jakůbek, T. Holý, S. Pospíšil, in: M. Barone, et al. (Eds.), A Portable Pixel Detector Operating as an Active Nuclear Emulsion and its Application for X-ray and Neutron Tomography, World Scientific, Singapore 2006, in print. Available on-line at ⟨http://villaolmo.mib.infn.it/ICATPP9th_2005/⟩.